CHINESE JOURNAL OF PHYSICS

https://www.journals.elsevier.com/chinese-journal-of-physics

IMPACT FACTOR = 3.237

Accepted April 8th 2022

MOMENT ANALYSIS OF UNSTEADY BI-COMPONENT SPECIES (DRUG) TRANSPORT WITH COUPLED CHEMICAL REACTION IN NON-NEWTONIAN BLOOD FLOW

O. Anwar Bég[1] and Ashis Kumar Roy[2,*]

[1]Professor and Director-Multi-Physical Engineering Sciences Group, Mechanical Engineering Department, School of Science, Engineering and Environment (SEE), University of Salford, Manchester, M54WT, **UK**

[2]Department of Science and Humanities, Tripura Institute of Technology, Narsingarh, Tripura -799009, **India.**

[*] *Author to whom correspondence should be addressed: Email: rk.ashis10@gmail.com (Ashis Kumar Roy)*

Abstract: Motivated by exploring the fluid dynamics of dual drug delivery systems in biomedicine, a mathematical analysis of the bi-component species transport (convective-diffusion) in rheological blood flow with bulk chemical reaction through a two-dimensional rigid vessel is presented. Two different bulk degradation reaction rates are included for the dual species (pharmacological agents, *A*, *B*). An analytical expression for axial velocity is derived using a perturbation method. The decoupled convection-diffusion equations are then analysed with the Aris – Barton approach. The mean concentration of the species is estimated using the first five concentration moments with the aid of fourth order Hermite polynomials. A finite difference technique based on the Crank Nicholson implicit scheme is employed to handle the p^{th} order moment of the general concentration. The analysis reveals that increasing reversible transfer rate and irreversible bulk degradation result in a reduction in the total mass of the species over time. The mass of both species decreases with an increase in reversible transfer rate, even though the mass of species *A* depletes faster than the mass of species *B*. The skewness of the concentration distribution decreases as yield stress increases and the distributions in all scenarios are positively skewed and tend to zero over time, implying that the distribution tends to symmetry over time. The kurtosis decreases over time from positive to negative values and eventually approaches zero. Mean concentration peaks for both species *A* and *B* are elevated with increasing yield stress, although magnitudes are significantly higher for species *A*. With increasing values of the distribution coefficient between two species, mean concentration peaks are elevated for species (component) *A* whereas they are depleted for species *B*, although substantially greater magnitudes are computed for species *B*. Good correlation of the skewness with earlier Newtonian results is achieved. The results provide some useful insight into the bi-component drug transport in smaller vessel pharmacodynamics where hemorheology is important.

Keywords: *Pharmacodynamics; irreversible bulk degradation; Aris-Barton method; perturbation solutions; Crank Nicolson numerics; skewness and kurtosis.*

1.Introduction

Hydrodynamic dispersion [1] is a fundamental area of modern fluid dynamics and arises in many areas of industrial technology, biomedicine and environmental sciences. It involves both molecular diffusion and convective dispersion (or mechanical dispersion). Important applications include chromatography, packed bed reactors and contaminant fate in geological transport. Another significant area of interest is *drug delivery* (pharmacodynamics) in which the fate of drugs introduced into the human body may be simulated with dispersion models. In recent years mathematical modelling of dispersion in medical fluid dynamics has received significant attention due to emerging applications in, for example, transport phenomena of therapeutic agents through neural tissues [2], nasal airway fluid dynamics [3], drug interaction with capillary blood flows [4], delivery of doxorubicin to hepatoma in pharmaceutical delivery [5], intercranial pharmacological flows [6] and tumour therapy [7,8]. Broneus *et al.* [9] reported on detailed experiments to determine the diffusivity of local anaesthetic drugs including hydrochloride salts of bupivacaine, etidocaine, lidocaine, mepivacaine, prilocaine and ropivacaine. Tripathi *et al.* [10] reviewed recent developments in computational hemodynamic models of nanoparticle-based pharmacological agents dispersing in streaming blood. An excellent appraisal of convective-diffusive transport relevant to hydrodynamic dispersion in blood flows was presented by Aroesty and Gross [11].

The above studies were generally confined to *Newtonian* blood flows especially in smaller vessels (at high shear rate blood typically acts like a Newtonian fluid as observed in large arteries). However the presence of numerous suspensions in blood including as erythrocytes (also known as RBC), leukocytes (WBC), thrombocytes, lymphocytes and lipoproteins suspended in a continuous saline plasma, render the nature of blood to be *non-Newtonian* [12]. Hemo-rheological models are therefore needed to correctly characterize blood in capillary transport and the rheological characteristics can have a dramatic effect on the efficacy of drug transport [13]. Many different non-Newtonian models have therefore been explored in hemodynamic transport (with and without drug dispersion) in recent years. Bég *et al.* [14] used a variational finite element code and the Nakamura-Sawada bi-viscosity model to simulate the drug diffusion in blood flow in tissue under an external magnetic field. Vita *et al.* [15] deployed a power-law (pseudoplastic/dilatant) model to compute 3-dimensional pulsatile blood flow in an aortic mechanical valve, also considering hemolysis. Antonova *et al.* [16] utilized both power law and Herschel-Bulkley (HB) yield stress non-Newtonian models to study

microvascular tone regulation in diabetes mellitus. Dubey *et al.* [17] used FREEFEM++ finite element software to analyze the two-dimensional nano-particle drug delivery in blood flow through a stenotic and aneurysmic arterial segment. They employed a Casson (viscoplastic) fluid model in the core region and the Sisko (viscoelastic) fluid model in the peripheral (porous) region. Chaturani and Palanisamy [18] used Eringen's micropolar model to study the pulsatile blood flow in a stenosed vessel. They deployed finite Hankel and Laplace transforms to derive closed-form expressions for axial and particle angular velocities, wall shear stress, resistance to flow and apparent viscosity. They also showed both inverse Fahraeus-Lindqvist and Fahraeus-Lindqvist effects are correctly captured with the micropolar non-Newtonian model. Vasu *et al.* [19] also implemented the Eringen micropolar model to compute the time-dependent nano-pharmacodynamic transport in a tapered stenotic vessel. Other non-Newtonian models which have been employed to analyse blood flow include Jeffery's viscoelastic model [20], the generalized Oldroyd-B fluid model [21] and the modified *Herschel*-Bulkley model [18,22].

As noted earlier, hydrodynamic dispersion is fundamental to drug delivery simulations. The original Taylor dispersion model [23] provides a robust platform for evaluating the *longitudinal* mean concentration (of, for example pharmacological agents) leading to a Gaussian distribution. In the Taylor approach, for large times, the mean concentration satisfies a one-dimensional diffusion-like equation. However, for evaluating the radial (transverse) concentration distribution, modified approaches are needed. Taylor's model has therefore been extended and refined by Gill (method of mean concentration expansion) [24] and Gill and Sankarasubramanian [25] so that the entire dispersion process (transverse and longitudinal) may be described in terms of a simple diffusion process with the effective diffusion coefficient as a function of time. Grotberg *et al.* [26] examined gas contaminant movement in pulmonary respiratory flows. Cirpka *et al.* [27] applied a modified Taylor dispersion model to solute transport in unsaturated heterogenous porous geological media. In the context of *non-Newtonian blood flows*, Dash *et al*. [28] used the generalized Gill-Sankarasubramanian model to study solute dispersion in viscoplastic (Casson) blood flow in a tube. They showed that dispersion rate (and effective diffusivity) is decreased with increasing yield stress of the fluid. They further showed that effective diffusivity is enhanced with time, although it achieves the steady state value below a critical time. They also identified that the location of the center of mass of a passive species over a cross section is not affected during the course of dispersion

and for different values of the plug flow parameter (i.e., the yield stress of the fluid). Barik and Dalal [29] used a homogenization technique (with up to up to third-order approximation) to study the two-dimensional concentration distribution in an oscillatory Couette flow. They observed that concentration variation rate over the channel cross-section is greater for thicker Stokes boundary layers and the dispersion of solute is elevated with an increment in Stokes boundary layer thickness.

The above studies generally ignored chemical reaction effects. These are known to be important in numerous haematological processes including coagulation [30,31], nitric oxide and S-nitrosohemoglobin interaction in hemo-regulation [32], venous flap flow regulation [33], multivalency counterbalancing in nano-drug delivery [34] and biochemistry of thrombosis [35,36]. Hathock [37] has identified that hemodynamic forces both control the predilection of specific anatomic sites to thrombosis and in addition greatly modify the biochemical reaction pathways involved in thrombus formation. Furthermore, thrombosis occurs in a dynamic *non-Newtonian* environment where flow conditions strongly influence the transport of coagulation factors, inhibitors, and cells. These observations support the need for computational and analytical investigations of *chemically reactive hemodynamic flow and dispersion with rheological models*, as considered in the present study. Several investigators have also reported results concerning dispersion in *Newtonian* blood flow with wall reactions. Lau and Ng [38] used a Flux Corrected Transport Algorithm (FCTA) and reactive boundary conditions to investigate the combined effects of reversible and irreversible wall reactions on the early development of the dispersion coefficient in convection-diffusion transport of a chemical species in steady flow through a small-diameter tube. Other Newtonian studies include Ng [39] (oscillatory tube flow), Paul and Mazumder (transient flow in an annular and tubular geometry) [40,41], Mazumder and Paul [42] and Roy *et al.* [43] (dispersion of reactive species in a non-Darcy porous medium). More recently reactive dispersion in non-Newtonian blood flow has also been analyzed. Roy *et al.* [44] studied the time-dependent dispersion of a passive contaminant of solute released in Casson viscoplastic tubular blood flow with a chemically active tube wall under a constant pressure gradient. They computed the transport coefficients, with the Aris-Barton moment technique and used a finite difference implicit scheme. They observed that convection coefficient and dispersion coefficient are inversely proportional to the yield stress, exchange coefficient is independent of yield stress and transport coefficients are significantly modified by wall absorption. Roy and Bég [45] used the Gill decomposition

method to compute the concentration of a reactive diffusing species in two fluid (Newtonian peripheral layer/micropolar core) hemodynamics in a rigid artery under constant axial pressure gradient with first-order chemical reaction. They showed that transverse concentration is enhanced with greater micropolar coupling number and reaction rate whereas it is suppressed with greater micropolar material parameter and peripheral to core viscosity ratio. They also observed that axial mean concentration peaks are decreased and migrate further along with the arterial geometry with greater micropolar material parameter values, whereas the converse behaviour is computed with higher micropolar coupling number.

Inspection of the literature has identified that the vast majority of studies communicated consider only a *single diffusing agent*. However increasingly pharmacological scientists are utilizing multiple drugs simultaneously. Therefore, it is important to *extend previous studies of hydrodynamic dispersion in non-Newtonian blood flow with chemical reactions, to consider two species (two different pharmacological agents). This is the focus of the present study*. Bi-compnent species diffusion has been examined theoretically in environmental contamination by Zeng *et al.* [46] and Gjetvaj *et al*. [47] again for *Newtonian* liquids. Clinical studies of dual species drug diffusion have been presented by Ganesan *et al.* [48], Taylor and Zografi [49] (for poly(vinylpyrrolidone) and indomethacin), Lloyd *et al.* [50] (for paracetamol and polyethylene glycol 4000 interaction), and Berthold *et al.* [51] (for nitric oxide and endogenous vasoconstrictor chemical interaction in renal blood flow regulation).

In the present article, *bi-component species (dual drug) convective-diffusion transport in non-Newtonian blood flow with bulk chemical reaction through a two-dimensional rigid vessel* is studied theoretically and numerically. The robust yield stress Casson fluid model is utilized. Two different bulk degradation reaction rates are included for the dual species (pharmacological agents, *A, B*). The governing species concentration equations are transformed to non-dimensional form with appropriate boundary conditions. An analytical expression for axial velocity is derived using a perturbation method. The decoupled convection-diffusion equations are then analyzed with the Aris – Barton approach, in which the p^{th} order moment of the general concentration is defined. The mean concentration of the species is estimated using the first five concentration moments with the aid of fourth order Hermite polynomials. A finite difference method based on the Crank Nicholson implicit scheme is employed to handle the p^{th} order moment of the general concentration. A statistical analysis is also conducted on the species transport. Coefficients of skewness and kurtosis are computed to determine the

symmetry and peaks of the concentration distribution. The computations may provide a deeper insight into dual drug behaviour in coagulating hemodynamics.

2.Reactive bi-component (dual drug) dispersion blood flow model

Dispersion model

Figure 1 illustrates the regime under consideration.

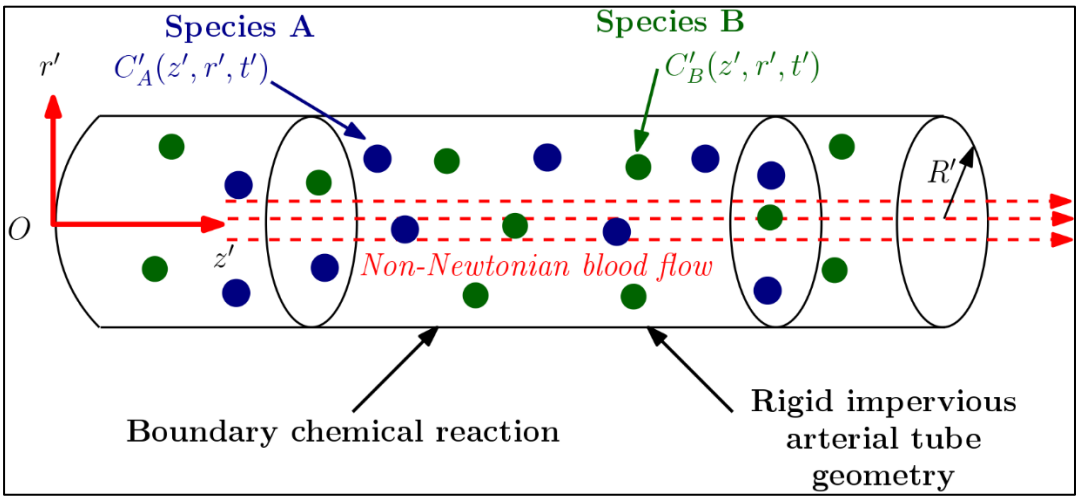

Fig. 1. Reactive two-component species dispersion in non-Newtonian blood flow

Two completely miscible and different reactive species (pharmacological agents, *A*, *B*) with concentration $C'_A(z',r',t')$. and $C'_B(z',r',t')$ are injected in a fully developed *unsteady* incompressible blood flow in a rigid cylindrical vessel. Here blood is simulated by the Casson model [18], which is a popular and accurate yield stress non-Newtonian model in hemodynamics. The governing species conservation equations for the two pharmacological agents (solutes) *A*, *B*, with coupled competitive reactions are:

$$\frac{\partial C'_A}{\partial t'}+u'(r',t')\frac{\partial C'_A}{\partial z'}=D'\frac{\partial^2 C'_A}{\partial z'^2}+\frac{D'}{r'}\frac{\partial}{\partial r'}\left(r'\frac{\partial C'_A}{\partial r'}\right)-r'_A\left(C'_A-k_dC'_B\right)-k'_AC'_A \quad \text{in} \quad 0<r'<R', \tag{1}$$

$$\frac{\partial C'_B}{\partial t'}+u'(r',t')\frac{\partial C'_B}{\partial z'}=D'\frac{\partial^2 C'_B}{\partial z'^2}+\frac{D'}{r'}\frac{\partial}{\partial r'}\left(r'\frac{\partial C'_B}{\partial r'}\right)+\frac{r'_B}{k_d}\left(C'_A-k_dC'_B\right)-k'_BC'_B \quad \text{in} \quad 0<r'<R', \tag{2}$$

here D' denotes constant molecular diffusivity of the species, r'_A is the transfer rate of species A, r'_B is the transfer rate of the species B, k_d is the distribution of coefficient between two species, k'_A and k'_B are the bulk degradation rate of the species A and B in the blood flow.

It is assumed that both neither *blood nor either of the two solutes, A, B* cannot penetrate the blood vessel, therefore,

$$\frac{\partial C'_A}{\partial r'} = \frac{\partial C'_B}{\partial r'} = 0 \qquad \text{at} \quad r' = R', \tag{3}$$

Again, the *symmetry condition* at the center of the blood vessel is read as:

$$\frac{\partial C'_A}{\partial r'} = \frac{\partial C'_B}{\partial r'} = 0 \qquad \text{at} \quad r' = 0. \tag{4}$$

It is assumed that both the species of equal mass *M* are released instantaneously in the blood flow at a time

$$C'_A(z', r', t') = C'_B(z', r', t') = \frac{M\delta(z')}{\pi R'^2}, \tag{5}$$

The upstream and downstream conditions for both the species *A and B* are:

$$C'_A(\pm\infty, r', t') = C'_B(\pm\infty, r', t') = 0. \tag{6}$$

Next the problem can be scaled using the following variables:

$$\begin{gathered} t = \frac{D't'}{R'^2}, \qquad r = \frac{r'}{R'}, \qquad z = \frac{D'z'}{R'^2U}, \quad C_A = \frac{\pi R'^3 C'_A}{M}, \quad C_B = \frac{\pi R'^3 C'_B}{M}, \\ r_A = \frac{r'_A R'^2}{D'}, \quad r_B = \frac{r'_B R'^2}{D'}, \quad k_A = \frac{k'_A R'^2}{D'}, \quad k_B = \frac{k'_B R'^2}{D'}, \qquad u = \frac{u'}{U}, \end{gathered} \tag{7}$$

Introducing Eqn. (7) into Eqs. (1) – (6) the model reduces to:

$$\frac{\partial C_A}{\partial t} + u(r,t)\frac{\partial C_A}{\partial z} = \frac{1}{\mathrm{Pe}^2}\frac{\partial^2 C_A}{\partial z^2} + \frac{1}{r}\frac{\partial}{\partial r}\left(r\frac{\partial C_A}{\partial r}\right) - r_A\left(C_A - k_d C_B\right) - k_A C_A \quad \text{in} \quad 0 < r < 1, \tag{8}$$

$$\frac{\partial C_B}{\partial t} + u(r,t)\frac{\partial C_B}{\partial z} = \frac{1}{\mathrm{Pe}^2}\frac{\partial^2 C_B}{\partial z^2} + \frac{1}{r}\frac{\partial}{\partial r}\left(r\frac{\partial C_B}{\partial r}\right) + \frac{r_B}{k_d}\left(C_A - k_d C_B\right) - k_B C_B \quad \text{in} \quad 0 < r < 1, \tag{9}$$

$$\frac{\partial C_A}{\partial r} = \frac{\partial C_B}{\partial r} = 0 \qquad \text{at} \quad r = 0,1, \tag{10}$$

$$C_A(z, r, 0) = C_A(z, r, 0) = \delta(z)/\mathrm{Pe}, \tag{11}$$

$$C_A(\pm\infty, r, t) = C_B(\pm\infty, r, t) = 0. \tag{12}$$

Equation (8) and (9) are *coupled* equations, and in order to decouple them the following transformations are used.

$$C_A(z, r, t) = -\frac{k_d}{r_B(\lambda_1 - \lambda_2)}\left[(r_A + k_A + \lambda_2)\Omega_A(z, r, t) - (r_A + k_A + \lambda_1)\Omega_B(z, r, t)\right], \tag{13}$$

$$C_B(z,r,t)=\frac{1}{\lambda_1-\lambda_2}\left[\Omega_A(z,r,t)-\Omega_B(z,r,t)\right], \tag{14}$$

where,

$$2\lambda_1=\sqrt{(r_A+r_B+k_A+k_B)^2-4(r_Ak_B+r_Bk_A+k_Ak_B)}-(r_A+r_B+k_A+k_B), \tag{15}$$

$$2\lambda_2=-\sqrt{(r_A+r_B+k_A+k_B)^2-4(r_Ak_B+r_Bk_A+k_Ak_B)}-(r_A+r_B+k_A+k_B), \tag{16}$$

Using Eqs. (13) and (14), the convective-diffusive dispersion problem becomes:

$$\frac{\partial\Omega_A}{\partial t}+\mathrm{Pe}\,u(r,t)\frac{\partial\Omega_A}{\partial z}=\frac{\partial^2\Omega_A}{\partial z^2}+\frac{1}{r}\frac{\partial}{\partial r}\left(r\frac{\partial\Omega_A}{\partial r}\right)+\lambda_1\Omega_A \quad \text{in} \quad 0<r<1, \tag{17}$$

$$\frac{\partial\Omega_B}{\partial t}+\mathrm{Pe}\,u(r,t)\frac{\partial\Omega_B}{\partial z}=\frac{\partial^2\Omega_B}{\partial z^2}+\frac{1}{r}\frac{\partial}{\partial r}\left(r\frac{\partial\Omega_B}{\partial r}\right)+\lambda_2\Omega_B \quad \text{in} \quad 0<r<1, \tag{18}$$

$$\frac{\partial\Omega_A}{\partial r}=\frac{\partial\Omega_B}{\partial r}=0 \qquad \text{at} \quad r=0,1, \tag{19}$$

$$\Omega_A(z,r,0)=\frac{\delta(z)}{\mathrm{Pe}}\left(\frac{r_B}{k_d}+r_A+k_A+\lambda_1\right), \tag{20}$$

$$\Omega_B(z,r,0)=\frac{\delta(z)}{\mathrm{Pe}}\left(\frac{r_B}{k_d}+r_A+k_A+\lambda_2\right), \tag{21}$$

$$\Omega_A(\pm\infty,r,t)=\Omega_B(\pm\infty,r,t)=0. \tag{22}$$

Further the following transformations are introduced:

$$\Omega_A=\left(\frac{r_B}{k_d}+r_A+k_A+\lambda_1\right)\Theta_A, \tag{23}$$

$$\Omega_B=\left(\frac{r_B}{k_d}+r_A+k_A+\lambda_2\right)\Theta_B. \tag{24}$$

The system of Eqs. (17) – (22) transform to:

$$\frac{\partial\Theta_A}{\partial t}+u(r,t)\frac{\partial\Theta_A}{\partial z}=\frac{1}{\mathrm{Pe}^2}\frac{\partial^2\Theta_A}{\partial z^2}+\frac{1}{r}\frac{\partial}{\partial r}\left(r\frac{\partial\Theta_A}{\partial r}\right)+\lambda_1\Theta_A \quad \text{in} \quad 0<r<1, \tag{25}$$

$$\frac{\partial\Theta_B}{\partial t}+u(r,t)\frac{\partial\Theta_B}{\partial z}=\frac{1}{\mathrm{Pe}^2}\frac{\partial^2\Theta_B}{\partial z^2}+\frac{1}{r}\frac{\partial}{\partial r}\left(r\frac{\partial\Theta_B}{\partial r}\right)+\lambda_2\Theta_B \quad \text{in} \quad 0<r<1, \tag{26}$$

$$\frac{\partial\Theta_A}{\partial r}=\frac{\partial\Theta_B}{\partial r}=0 \qquad \text{at} \quad r=0,1, \tag{27}$$

$$\Theta_A(z,r,0)=\Theta_B(z,r,0)=\delta(z)/\mathrm{Pe}, \tag{28}$$

$$\Theta_A(\pm\infty, r, t) = \Theta_B(\pm\infty, r, t) = 0. \tag{29}$$

The *moment analysis* of the system (25)-(29) is addressed in due course.

Velocity solution

The constitute equation for Casson non-Newtonian fluid model is as follows:

$$\begin{cases} \boldsymbol{\tau} = \left(\sqrt{\mu} + \sqrt{\tau_y' / |\dot{\gamma}'|}\right)^2 \dot{\boldsymbol{\gamma}}' & \text{for } |\tau'| > \tau_y' \\ \dot{\boldsymbol{\gamma}}' = 0 & \text{for } |\tau'| \leq \tau_y' \end{cases} \tag{30}$$

where, $\dot{\boldsymbol{\gamma}}$ and $\boldsymbol{\tau}$ denotes the strain rate and stress tensor respectively, whereas τ_y' is the yield stress. The operator $|\cdot|$ used in Eq. (30) indicates the magnitude of the respective terms, μ is the viscosity.

For one dimension, shear flow is the constitutive Eq. (30) in *non-dimensional* form is:

$$-\frac{\partial u}{\partial r} = \begin{cases} \left[\sqrt{\tau} - \sqrt{\tau_y}\right]^2 & \text{for } \tau > \tau_y \\ 0 & \text{for } \tau \leq \tau_y \end{cases} \tag{31}$$

where $u = u'/U$ and $(\tau, \tau_y) = (\tau', \tau_y') / \mu(U / R')^n$.

The momentum equation in non-dimensional form with boundary conditions at the rigid wall and along the centreline of the tube are:

$$\frac{1}{\mathrm{Sc}} \frac{\partial u}{\partial t} = 2p(t) - \frac{1}{r} \frac{\partial}{\partial r}(r\tau), \tag{32}$$

$$\tau \text{ is finite at } r = 0, \tag{33}$$

$$u = 0 \text{ at } r = 1. \tag{34}$$

Here, $\mathrm{Sc} = \nu / D'$ is the Schmidt number and $p(t) = 2\left(1 + e\sin\alpha^2 \mathrm{Sc}\, t\right)$, α is known as Womersley frequency parameter (for pulsating blood flow). To solve the momentum equation, a perturbation method is utilized, considering $\grave{o} = 1/\mathrm{Sc}$ [52] as a small parameter accordingly, we expand the *velocity and the shear stress* in the following manner:

$$\tau(t, r) = \tau_0(t, r) + \grave{o}\tau_1(t, r) + \cdots \tag{35}$$

$$u(t, r) = u_0(t, r) + \grave{o}u_1(t, r) + \cdots \tag{36}$$

where,

$$\tau_0(t,r) = p(t)r \tag{37}$$

$$\tau_1(t,r) = -\frac{p'(t)}{2}\left[\frac{r}{2} - \frac{r^3}{4} + r_p\left(r - \frac{2}{3}r^2\right) - \sqrt{r_p}\left(\frac{4}{3}r - \frac{16}{21}r^{5/2}\right)\right] \tag{38}$$

and

$$u_0(t,r) = \frac{p(t)}{2}\left[\left(1-r^2\right) - \frac{8}{3}\sqrt{r_p}\left(1-r^{3/2}\right) + 2r_p\left(1-r\right)\right], \tag{39}$$

$$\begin{aligned} u_1(t,r) = &-\frac{p'(t)}{2}\left[\frac{3}{16} - \frac{r^2}{16}(4-r^2) - \frac{r_p^2}{16}\left(\frac{1144}{147} - \frac{16}{3}(r+r^{3/2}) + \frac{424}{147}r^{7/2}\right)\right] \\ &- \frac{p'(t)}{32}r_p\left(\frac{320}{63} + \frac{128}{63}r^{3/2} - \frac{64}{9}r^{3/2}\right). \end{aligned} \tag{40}$$

Here, r_p is the plug flow radius. For the *special case* of $r_p = 0$, then non-Newtonian Casson model [52] reduces to classical Newtonian model.

Moment analysis of species concentration

The *decoupled Convection-diffusion* for both the species have the same form (see Eqs. (25) and (26)), and thus we have dropped the subscript *A and B* for simplicity prior to applying the Aris – Barton [53] approach. The p[th] order moment of the general concentration $\Theta(z,r,t)$ is defined as:

$$\Theta_p(t,r) = \int_{-\infty}^{+\infty} z^p \Theta(t,r,z)dz \tag{41}$$

Here Θ_p is the solution of the following partial differential equation:

$$\frac{\partial \Theta_p}{\partial t} - \frac{1}{r}\frac{\partial}{\partial r}\left(r\frac{\partial \Theta_p}{\partial r}\right) - \lambda\Theta_p = pu(r)\,\Theta_{p-1} + \frac{p(p-1)}{\mathrm{Pe}^2}\Theta_{p-2} \tag{42}$$

$$\frac{\partial \Theta_p}{\partial r} = 0 \qquad \text{at} \quad r = 0,1, \tag{43}$$

$$\Theta_p(0,r) = \begin{cases} 1/\mathrm{Pe} & \text{for } p = 0 \\ 0 & \text{for } p > 0 \end{cases} \tag{44}$$

For future reference, the p[th] moment about the mean of the species concentration is presented below

$$\nu_p(t) = \frac{\int_0^1 \int_{-\infty}^{+\infty} r(z - z_g)^p \Theta \, \mathrm{d}r \, \mathrm{d}z}{\int_0^1 \int_{-\infty}^{+\infty} r \, \Theta \, \mathrm{d}r \, \mathrm{d}x} \tag{45}$$

Where

$$z_g = \frac{\int_0^1 \int_{-\infty}^{+\infty} r \, z \, \Theta \, \mathrm{d}r\mathrm{d}z}{\int_0^1 \int_{-\infty}^{+\infty} r \, \Theta \, \mathrm{d}r\mathrm{d}z} = \frac{\bar{\Theta}_1}{\bar{\Theta}_0} \tag{46}$$

Denotes the *centroid of the solute* and the over-bar denotes the *sectional average*. By simple manipulation, we get:

$$\nu_2(t) = \frac{\bar{\Theta}_2}{\bar{\Theta}_0} - z_g^2, \tag{47}$$

$$\nu_3(t) = \frac{\bar{\Theta}_3}{\bar{\Theta}_0} - 3z_g\mu_2 - z_g^3, \tag{48}$$

$$\nu_4(t) = \frac{\bar{\Theta}_4}{\bar{\Theta}_0} - 4z_g\mu_3 - 6z_g^2\mu_2 - z_g^4, \tag{49}$$

By using the first five concentration moments, we can estimate the mean concentration of the species $\bar{\Theta}$, using the fourth-order Hermite polynomials – see [54,55]

$$\bar{\Theta}(z,t) = \bar{\Theta}_0 \exp\left(\frac{z - z_g}{\sqrt{2\mu_2}}\right) \sum_{n=0}^{4} c_n(t) H_n\left(\frac{z - z_g}{\sqrt{2\mu_2}}\right) \tag{50}$$

Where,

$$c_0 = \frac{1}{\sqrt{2\pi\mu_2}}, c_1 = 0, c_2 = 0, c_3 = \frac{\sqrt{2}a_0\nu_2}{24}, c_4 = \frac{a_0\nu_3}{96} \tag{51}$$

and H_i is the Hermite polynomial satisfying following recurrence relation:

$$\left.\begin{aligned} H_{i+1}(\eta) = 2\eta H_i(\eta) - 2iH_{i-1}(\eta), \; i = 0,1,2,\ldots \\ H_0(\eta) = 1. \end{aligned}\right\}. \tag{52}$$

In the next section, we mainly investigate the various *statistical parameters* characterizing the solute transport. For this purpose, we define the following parameter $\varepsilon_r = r_B / r_A$ representing the *ratio of the reversible transfer rate of species B to that of species A*. In a similar fashion we

define $\varepsilon_k = k_B / k_A$ symbolising the ratio of irreversible degradation rate. First the *mass residual in the flow* is estimated and this is defined by the following relation:

$$M(t) = \begin{cases} \dfrac{\int_0^1 \int_0^\infty C_A(z,r,t)dzdr}{\int_0^1 \int_0^\infty C_A(z,r,0)dzdr} & \text{for species A} \\ \dfrac{\int_0^1 \int_0^\infty C_A(z,r,t)dzdr}{\int_0^1 \int_0^\infty C_A(z,r,0)dzdr} & \text{for species B} \end{cases} \tag{53}$$

The coefficients of skewness (β_2) and kurtosis (β_3) are critical determinants in the context of symmetry and peakedness of the concentration distribution. In order to determine whether the concentration curve deviates from the *normal curve*, these two parameters are required. When these two parameters have zero values, the distribution becomes *perfectly Gaussian*. The coefficients of skewness (β_2) and kurtosis (β_3) are defined respectively as:

$$\beta_2 = \frac{\nu_3}{\nu_2^{1.5}} \quad \text{and} \quad \beta_2 = \frac{\nu_4}{\nu_2^2} - 3 \tag{54}$$

3.Numerical Solution of Pth Order Moment General Concentration Equation

In order to solve Eq. (42) i.e., the pth order moment general concentration partial differential equation under boundary conditions (43) and (44), a finite difference method based on the Crank Nicholson implicit scheme is employed. Further details of numeric are given in [56,57]. In this technique, all the terms in Eq. (42) are defined at each node point (i, j), where i corresponds to time and j corresponds to space. For the spatial derivative and time derivative in Eq. (42) the following approximations are used:

$$\frac{\partial \Theta_p}{\partial t} = \frac{\Theta_p(i+1, j) - \Theta_p(i, j)}{\Delta t} \tag{55}$$

$$\frac{\partial \Theta_p}{\partial r} = \frac{\Theta_p(i+1, j+1) - \Theta_p(i+1, j-1) + \Theta_p(i, j+1) - \Theta_p(i, j-1)}{4\Delta r} \tag{56}$$

$$\frac{\partial^2 \Theta_p}{\partial r^2} = \frac{\Theta_p(i+1, j+1) - 2\Theta_p(i+1, j) + \Theta_p(i+1, j-1) + \Theta_p(i, j+1) - 2\Theta_p(i, j) + \Theta_p(i, j-1)}{2(\Delta r)^2} \tag{57}$$

The resulting finite difference equation turns into a system of a linear algebraic equation with a tri-diagonal coefficient matrix,

$$P_j \Theta_p(i+1, j+1) + Q_j \Theta_p(i+1, j) + R_j \Theta_p(i+1, j-1) = S_j \tag{58}$$

the associate initial and boundary condition becomes

$$\Theta_p(1, j) = \begin{cases} 1 & \text{for} \quad p = 0 \\ 0 & \text{for} \quad p > 0 \end{cases} \tag{59}$$

$$\Theta_p(i, 0) = \Theta_p(i, 2) \tag{60}$$

$$\Theta_p(i, M+1) = \Theta_p(i, M-1) \tag{61}$$

The above tri-diagonal system is solved by the Thomas algorithm. In the present computations, $M = 201$ and $\Delta t = 0.00001$. To select *M*, a mesh independence has been performed for steady dispersion coefficient (See Fig. 2). A MATLAB code has been prepared to solve Eq. (42) by using the above-mentioned method.

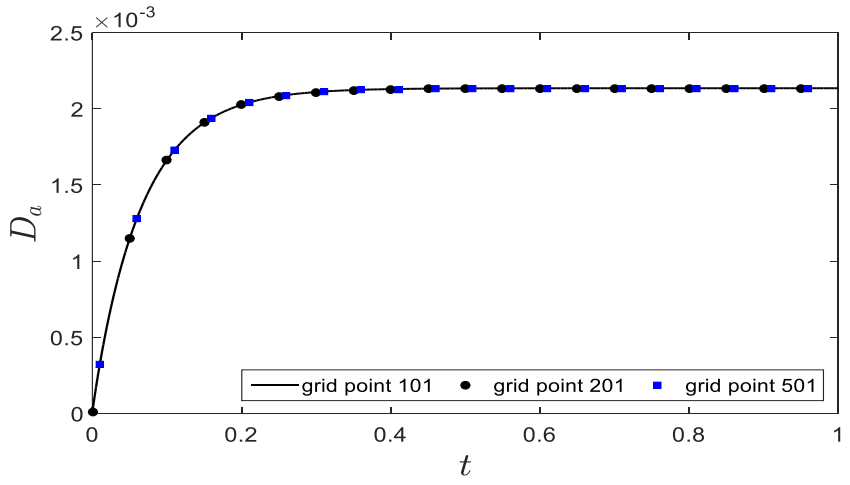

Fig. 2. Grid independent study for steady dispersion coefficient and fixed $\varepsilon_r = \varepsilon_k = 1$, $\alpha = 0.5$ and $k_d = 2$.

4.Result and discussion:

Figs. 3-10 visualize the results. All default data prescribed in the analysis is given in the respective figure. The typical range of these parameter are taken from literature as given bellow:

Parameter	Range	Reference
k_d	0.5 – 8	[46]
ε_r	0.25 – 8	[46]
ε_k	0.25 – 8	[46]
τ_y	0 – 0.05	[28] , [44], [55]
α	0.05	[55], [58]
e	0 (steady) 1 (unsteady)	[58]

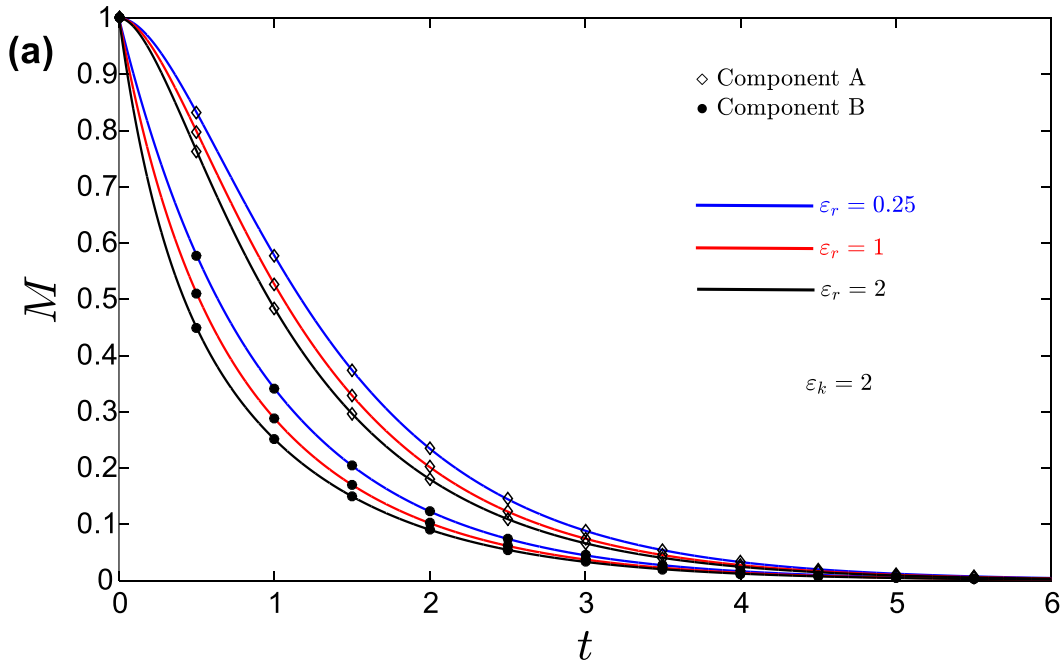

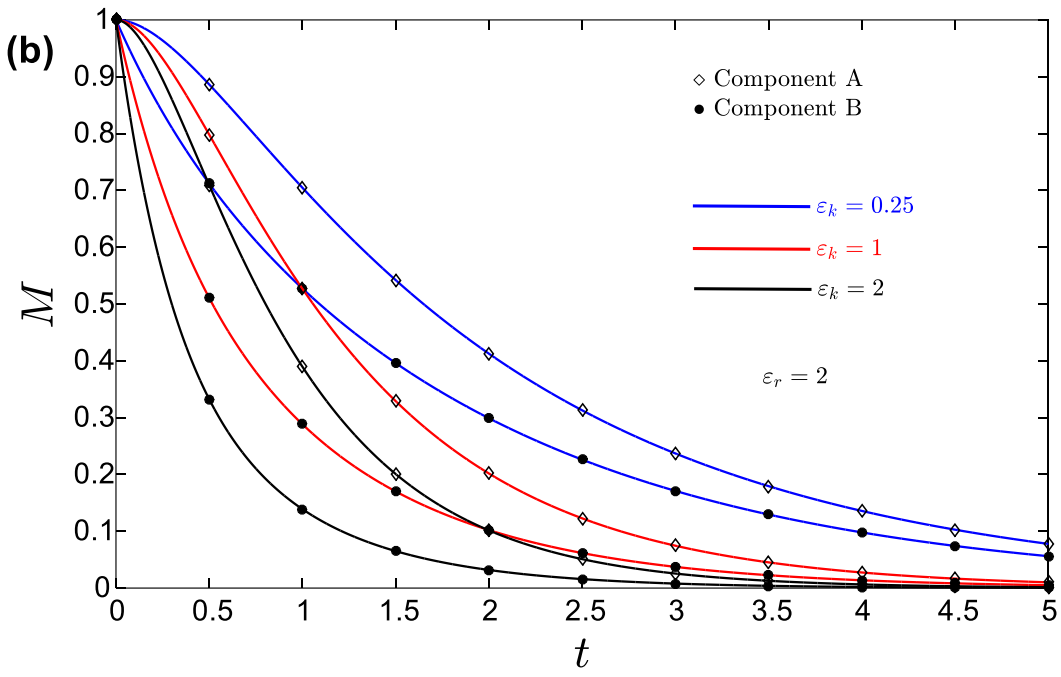

Fig. 3. Temporal evolution of solute residual in the flow for both the species (a) variety of ε_r and (b) for various ε_k with fixed $k_d = 2$.

Fig. 3 shows the evolution with time of the solute residual in the blood flow for both species for (a) various ε_r and (b) for various ε_k . In both plots the distribution of coefficient between two species *A and B* is set as $k_d = 2$. As expected, reversible transfer rate and irreversible bulk degradation deplete the total mass of the species over time. **Fig. 3a** shows that the mass of both species decreases with an increase in *reversible reaction rate* ε_r. In a similar fashion, mass decay happens rapidly with the increase of the ratio of irreversible degradation rate ε_k (**Fig. 3b**). It is also noteworthy that the mass of species *A* depletes faster than the mass of species *B* and this is intimately associated with the transfer rates of both species (r_A' , r_B'), bulk degradation rates of both species (k_A', k_B') and in particular the distribution of coefficient between two species, k_d . $k_d = 2$ indicating that species *A* dominates i.e., there is a faster conversion of this species compared with species *B*. The implication is that pharmacological agent reactions are controlled, among other factors by the *relative rates of bulk degradation* [48,49].

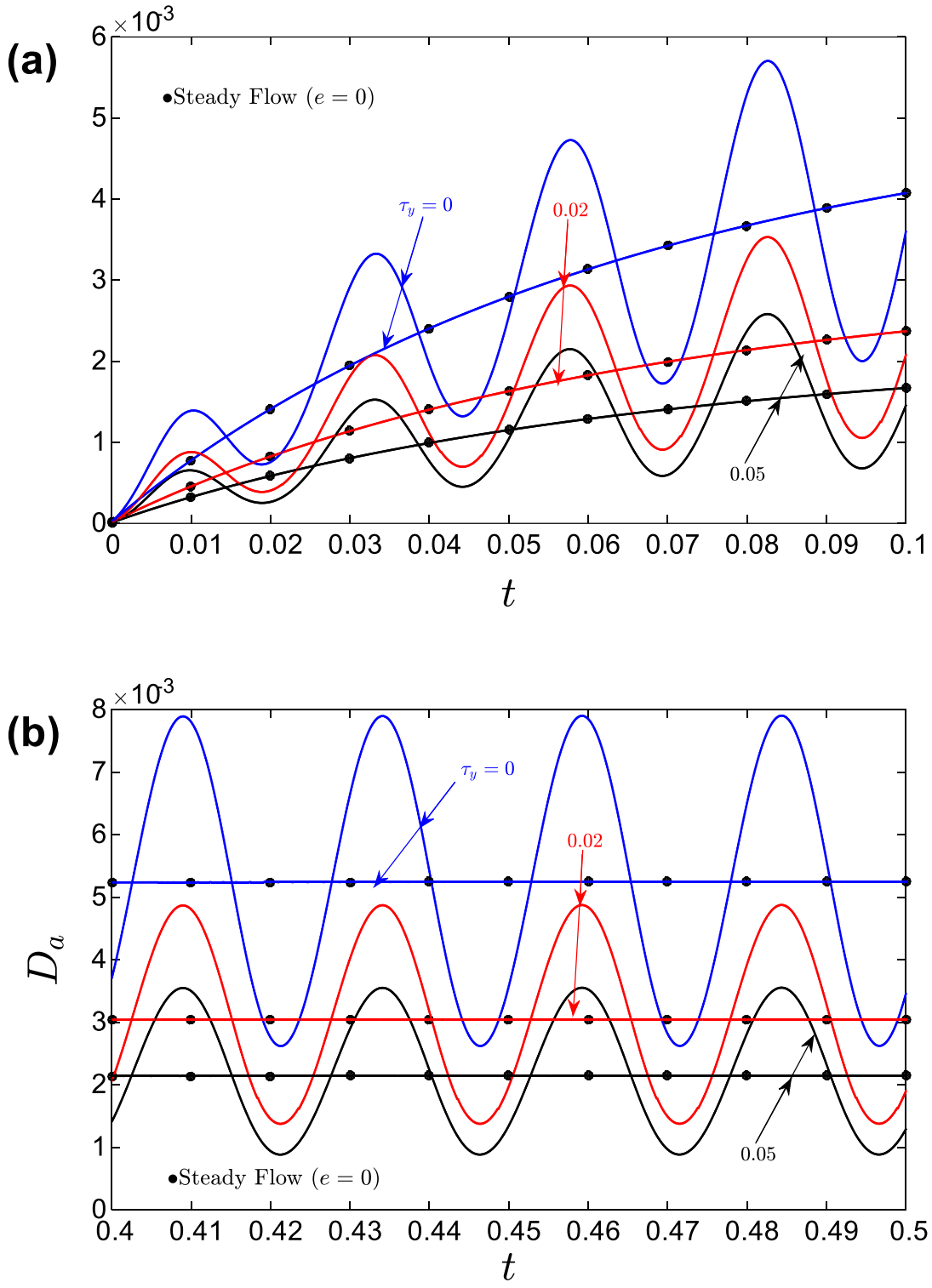

Fig. 4. Time-dependent dispersion coefficient of species *A* with (a) small and (b) large time for fixed $\varepsilon_r = \varepsilon_k = 1$, $\alpha = 0.5, e = 0.5, 0$ and different yield stress (τ_y).

Fig. 4a, b visualizes the *time-dependent dispersion coefficient* of species *A* with (a) small and (b) large time for fixed $\varepsilon_r = \varepsilon_k = 1$, $\alpha = 0.5, e = 0.5, 0$ and different yield stress (τ_y). It is evident that the *effective dispersion coefficient* defined by $D_a = 0.5\, d\nu_2 / dt$, for both species are approximately equal. Therefore, we restrict attention to consider one species i.e., *A*. In consistency with the available literature [54,58], the dispersion coefficient of species *A* exhibits a *pulsatile nature* (see **Fig 4a, b**). At *small times*, the *amplitude* of the dispersion curve is not uniform and it exhibits a growth; however, at *large time* (t>0.4), the amplitude of the dispersion curve becomes stable. Also, **Figs. 4a, b** both demonstrate that a higher yield stress (τ_y) suppresses the amplitude. This is attributable to the increase in plug radius with an increase in yield stress. This progressively reduces the shear flow regime (Stokes boundary layer) in the vicinity of the wall and hence decreases the effective dispersion coefficient.

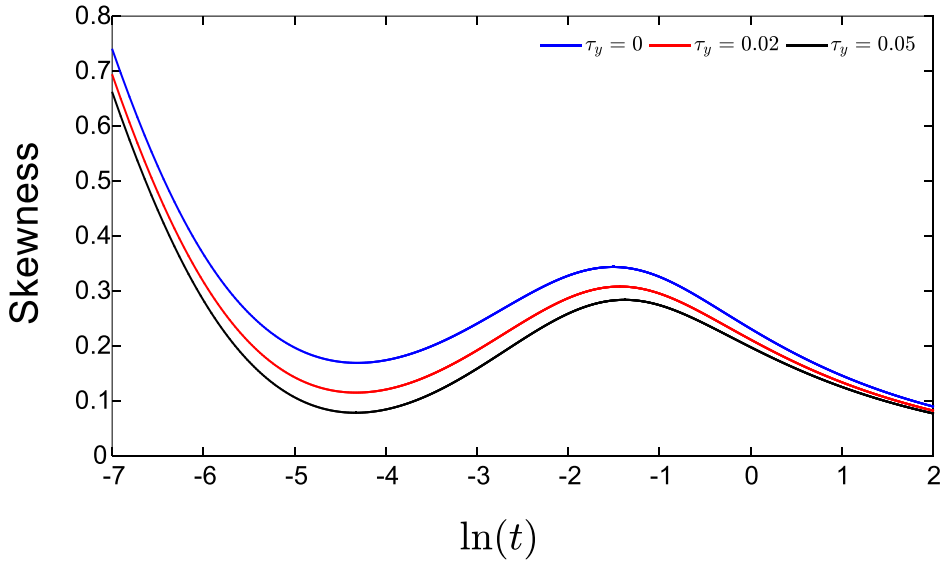

Fig. 5. Temporal evolution of skewness of the species for fixed $\varepsilon_r = \varepsilon_k = 1$, $k_d = 2$, $e = 0$ and different yield stress (τ_y).

Figure 5. displays the distribution over time of coefficient of skewness (β_2) of the species for fixed $\varepsilon_r = \varepsilon_k = 1$, $k_d = 2$, $e = 0$ and different yield stress (τ_y). As with dispersion coefficient, skewness exhibits a similar trend for both species *A and B*, and we confine ourselves to the species *A*. It is apparent that the parametric dependency of the dispersion coefficient remains the same regardless of the flow characteristics (steady, i.e., $e = 0$, or pulse, i.e., $e > 0$). As a

result, we limit ourselves to the *steady flow* scenario hereafter. The temporal evolution of skewness for steady flow $(e=0)$ displayed in **Fig. 5.** as a linear-*log* plot for all values of yield stress. The skewness topologies have a similar profile to the results of Wang and Chen [59], in the time range [0.1, 2] for the *Newtonian case* (zero yield stress). For t < 0.1, the skewness decreases and achieves its lowest value, subsequently increases then eventually decreases to zero with the progression of time. Additionally, the figure illustrates that with the increase of yield stress, skewness of the concentration distribution *decreases*. *The rheology of blood therefore exerts a significant effect on the skewness which cannot be captured with Newtonian models*. The Newtonian case (τ_y = 0) clearly achieves the *maximum skewness at all times*, whereas the strongly non-Newtonian case (τ_y = 0.05) produces the *minimum skewness* at any time. It is also worth noting that the distributions in all scenarios are *positively skewed* and tend to zero over time, implying that the distribution tends to symmetry over time.

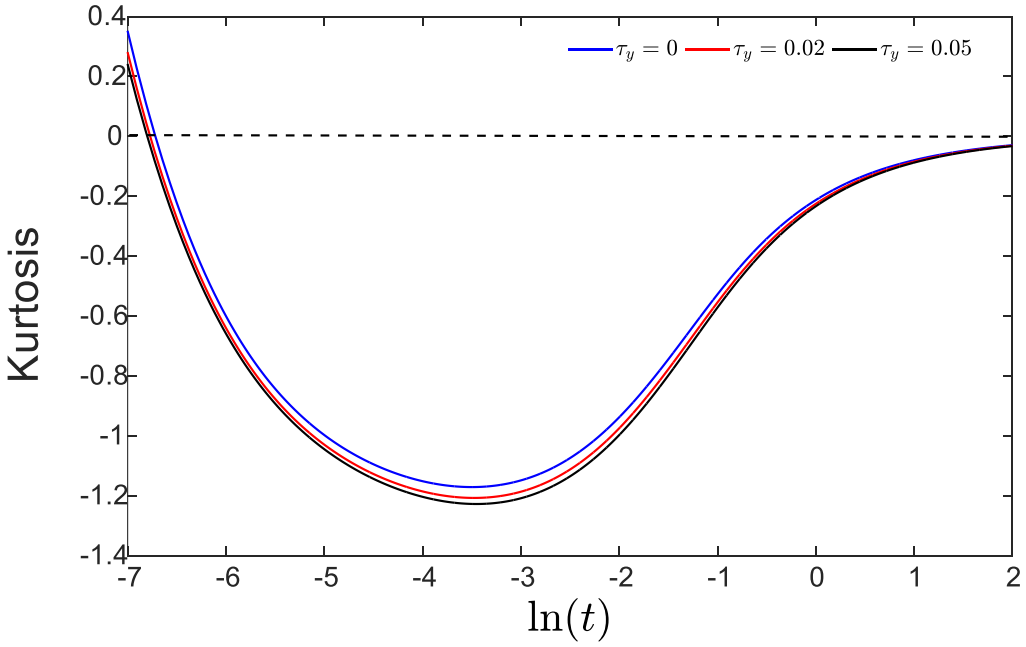

Fig. 6. Temporal evolution of kurtosis of the species for fixed $\varepsilon_r = \varepsilon_k = 1$, $k_d = 2$, $e = 0$ and different yield stress (τ_y).

Figure 6 depicts the temporal evolution of *coefficient of kurtosis* of the species, for fixed $\varepsilon_r = \varepsilon_k = 1$, $k_d = 2$, $e = 0$ and different yield stress (τ_y). While **skewness** quantifies the extent to which the concentration distribution is symmetrical, ***kurtosis*** is a measure of whether the distribution is too peaked (i.e., a very narrow distribution with the maximum concentrations in

in the centre). As noted earlier, kurtosis is a necessary complement to skewness. It is evident that kurtosis decreases over time from positive to negative values and eventually approaches zero. There is an initial critical time for each yield stress at which the kurtosis is zero; additionally, at large times, the kurtosis is also zero. This means that the distribution of the solute attains the Gaussian distribution at an initial critical time and also large time as well. The influence of yield stress is opposite to that computed for skewness. With increasing yield stress there is a distinct reduction in the coefficient of kurtosis. However, the effect is less prominent than for the skewness.

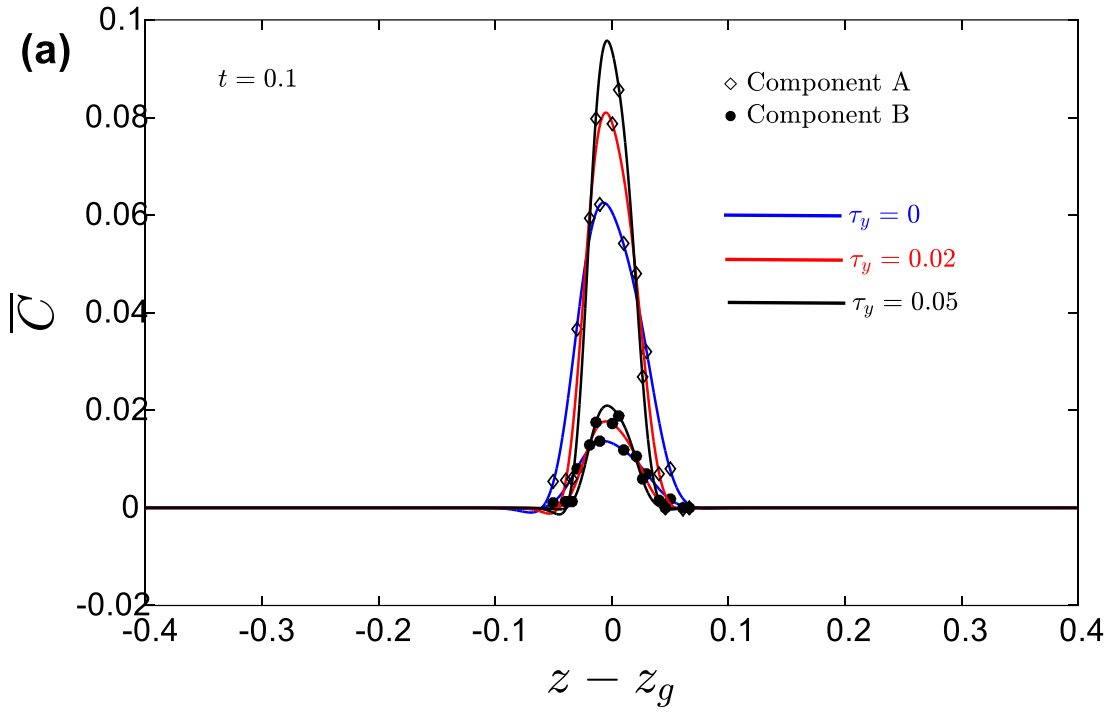

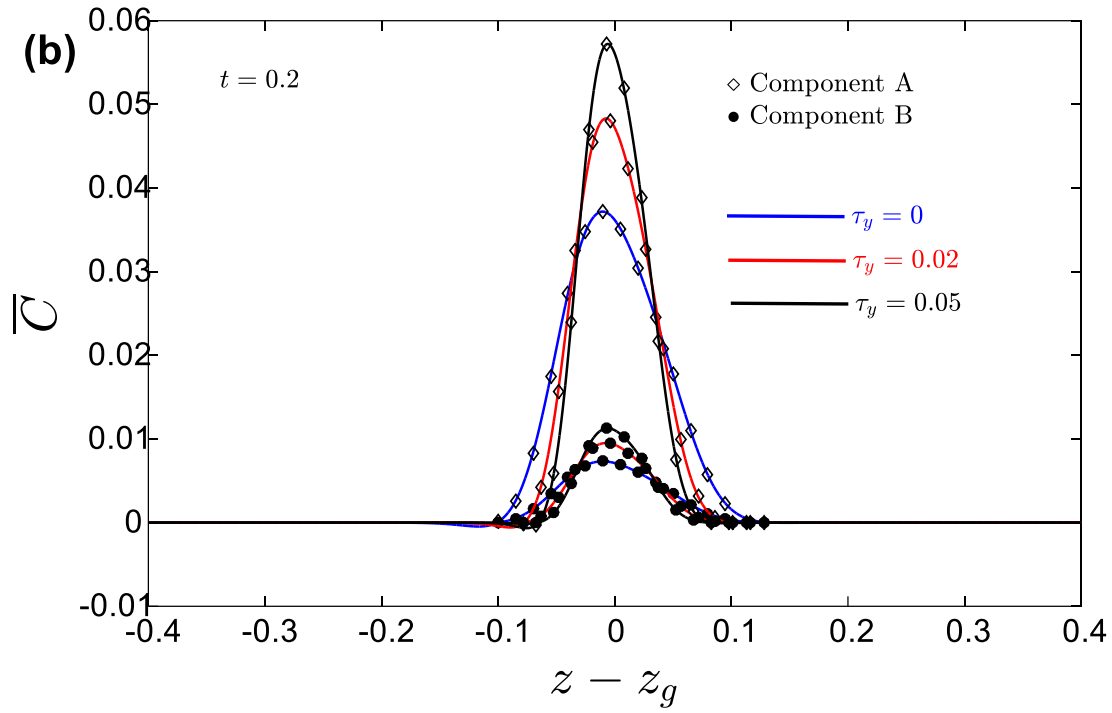
(b)
$t = 0.2$
◇ Component A
● Component B
$\tau_y = 0$
$\tau_y = 0.02$
$\tau_y = 0.05$
$|C|$
$z - z_g$

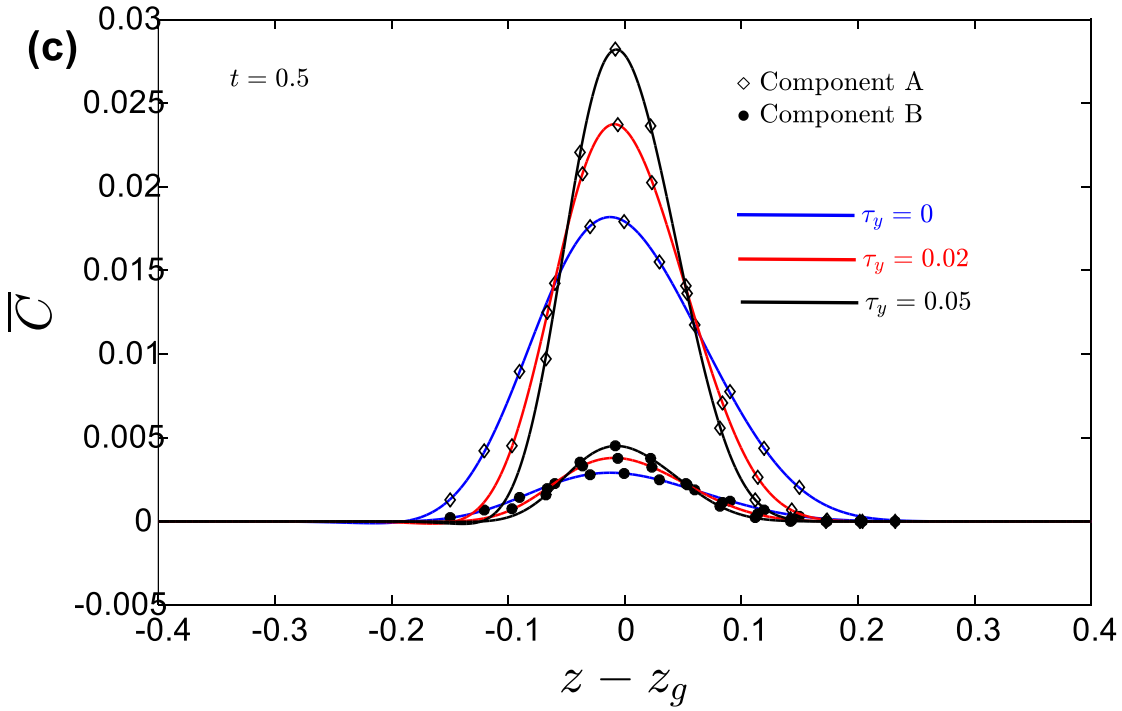
(c)
$t = 0.5$
◇ Component A
● Component B
$\tau_y = 0$
$\tau_y = 0.02$
$\tau_y = 0.05$
$|C|$
$z - z_g$

Fig. 7. mean concentration distributions for binary components at three different times and various yield stress (τ_y) with $\varepsilon_r = \varepsilon_k = 1,\ k_d = 2,\ e = 0$.

Figure 7a, b, c illustrates the mean concentration distributions $(\bar{C})$ for species *A*, *B* i.e., the binary components at three different times and various yield stress (τ_y) with $\varepsilon_r = \varepsilon_k = 1$, $k_d = 2,\ e = 0$. In all three figures it is evident that species *A* achieves significantly higher mean concentration $(\bar{C})$ than species *B*. There is however a progressively greater lateral spreading of the profiles with increasing time. This implies that as time elapses the magnitude of concentration distribution for species *A* becomes exceeded by species *B*. All three figures also show that with increasing yield stress (τ_y), generally the mean concentration $(\bar{C})$ is increased. Clearly therefore the Newtonian case (τ_y = 0) produces the *minimal* mean concentration whereas the strongly non-Newtonian case (τ_y = 0.05) produces the *maximum.* The implication is therefore that a *Newtonian model under-predicts* the actual mean concentration in the reactive dispersion in blood flow. This justifies the adoption of a non-Newtonian model since rheological effects clearly produce non-trivial modifications in the mean concentration distributions.

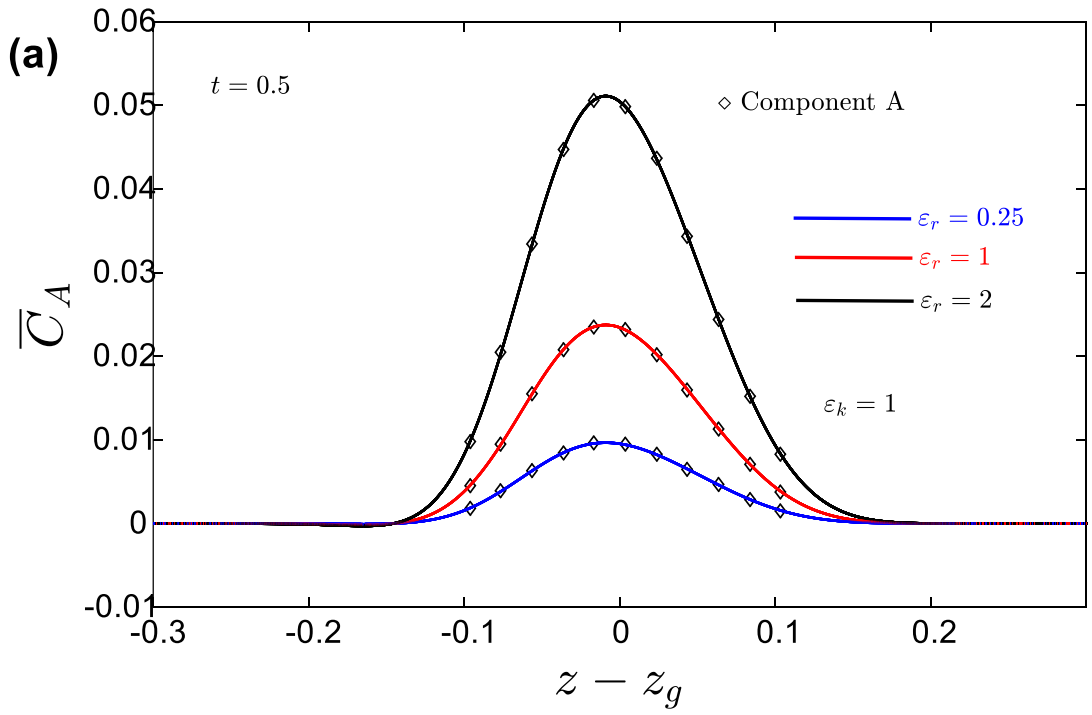

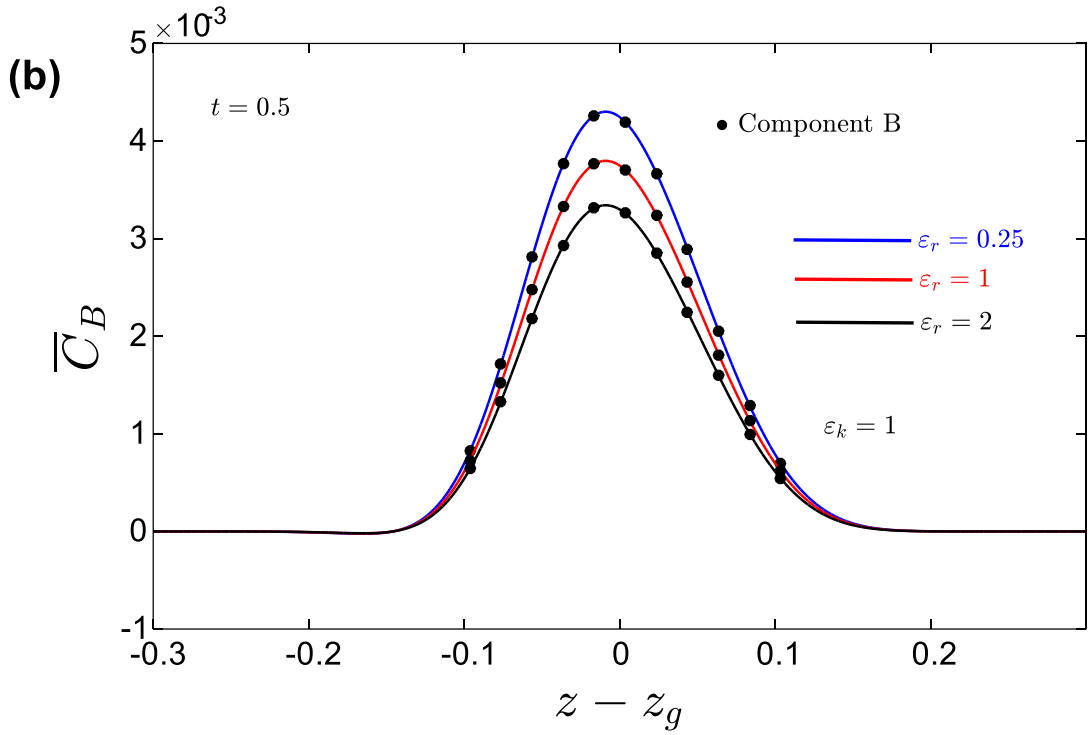

Fig. 8. Mean concentration distribution for species *A and B* for various ε_r with fixed $k_d = 2$.

Figure 8a, b illustrates the mean concentration distribution for individual species *A and B* for various values of ε_r i.e., the ratio of the reversible reaction rate of species *B* to that of species *A*. Again $k_d = 2$ and non-Newtonian blood is considered. Significantly higher magnitudes of $(\bar{C}_A)$ are observed in **Fig. 8a** compared with $(\bar{C}_B)$ (**Fig. 8b**). With increasing ε_r values there is a marked enhancement in $(\bar{C}_A)$ magnitudes; however, over the same increment in ε_r there is a depletion in $(\bar{C}_B)$ magnitudes. Clearly therefore the relative reaction rates of the two species exert a significant influence on the hydrodynamic dispersion phenomenon in blood flow. The efficacy of drugs (pharmacological agents) therefore can be manipulated with careful selection of their reaction rates [49].

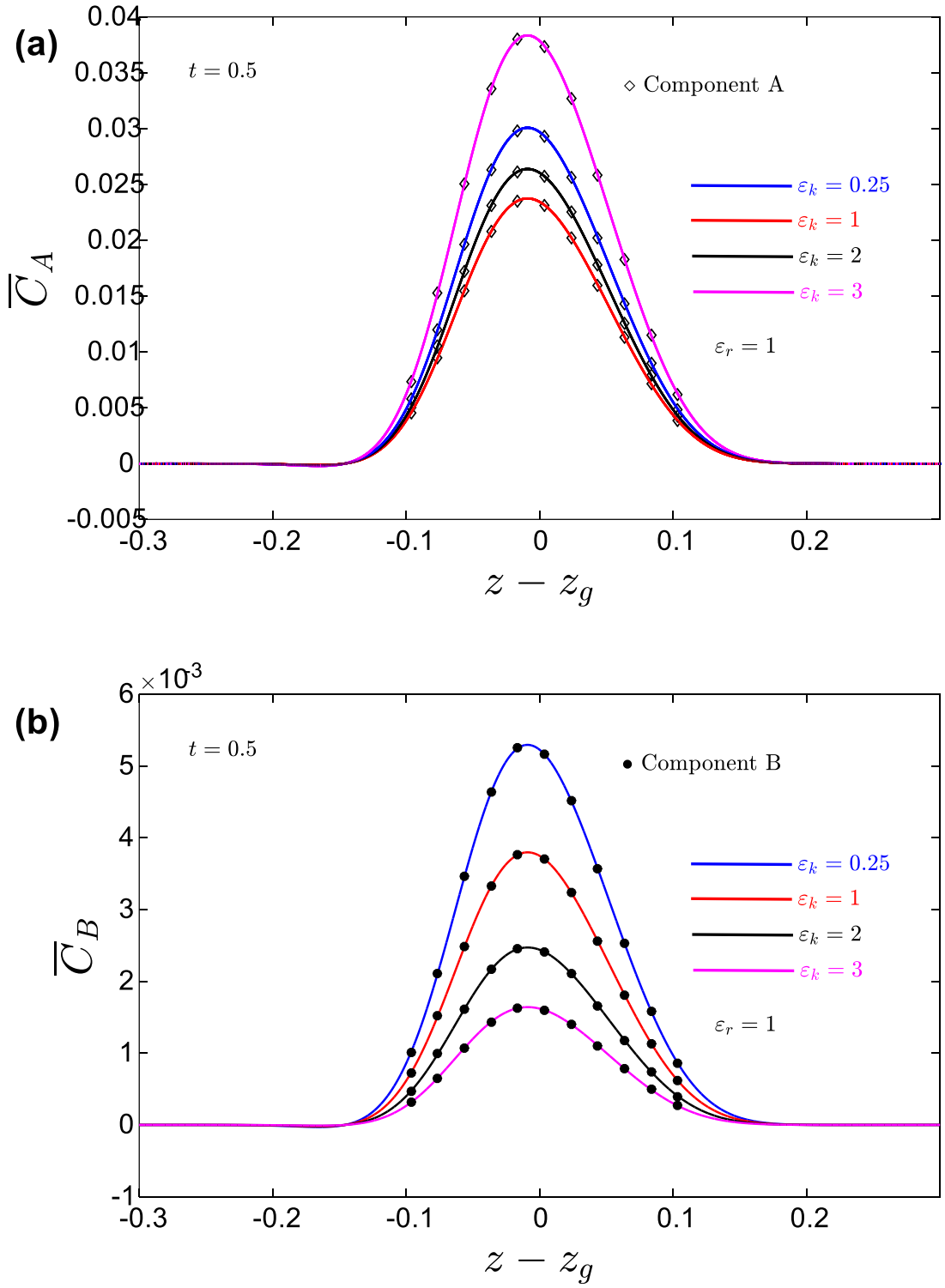

Fig. 9. Mean concentration distribution for species *A and B* for various ε_k with fixed $k_d = 2$.

Figure 9a, b illustrates the mean concentration distribution for individual species *A and B* for various values of ε_k i.e., the ratio of the ratio of irreversible degradation rate of species *B* to

that of species *A*. Again, distribution coefficient between the two species *A and B*, $k_d = 2$ and non-Newtonian blood is considered. There is a substantial accentuation in $\bar{C}_A$ magnitudes (**Fig. 9a**) with increasing ε_k values whereas there is a noticeable reduction in $\bar{C}_B$ magnitudes (**Fig. 9b**). The topology of either set of plots however is not significantly altered at any value of ε_k.

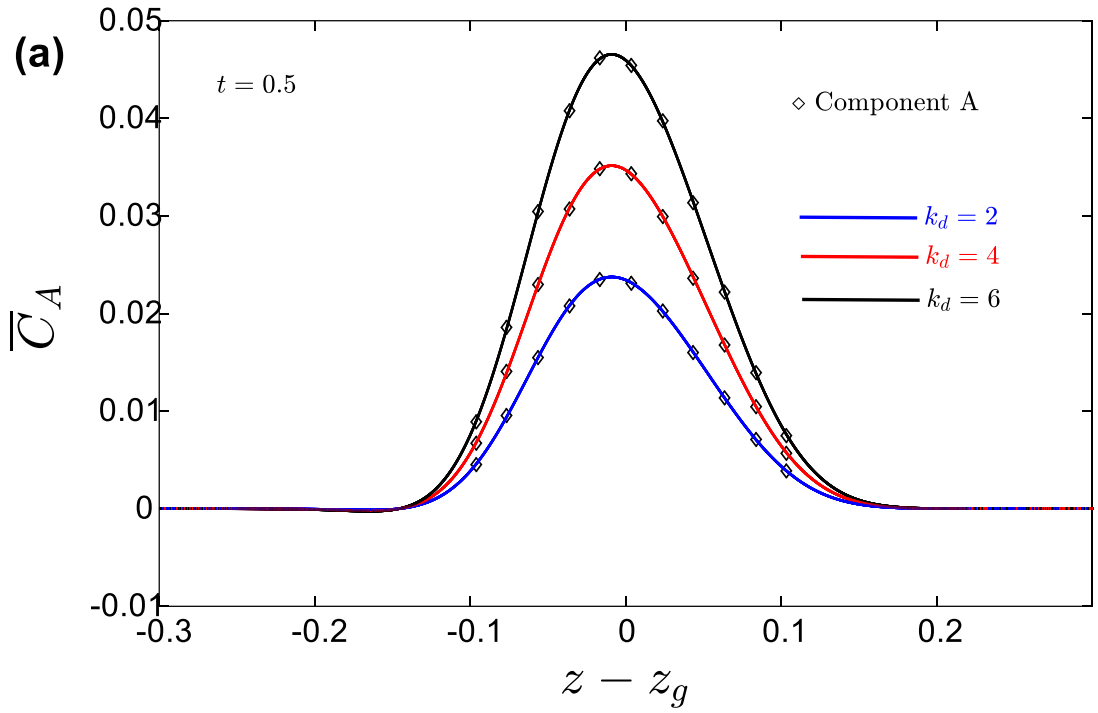

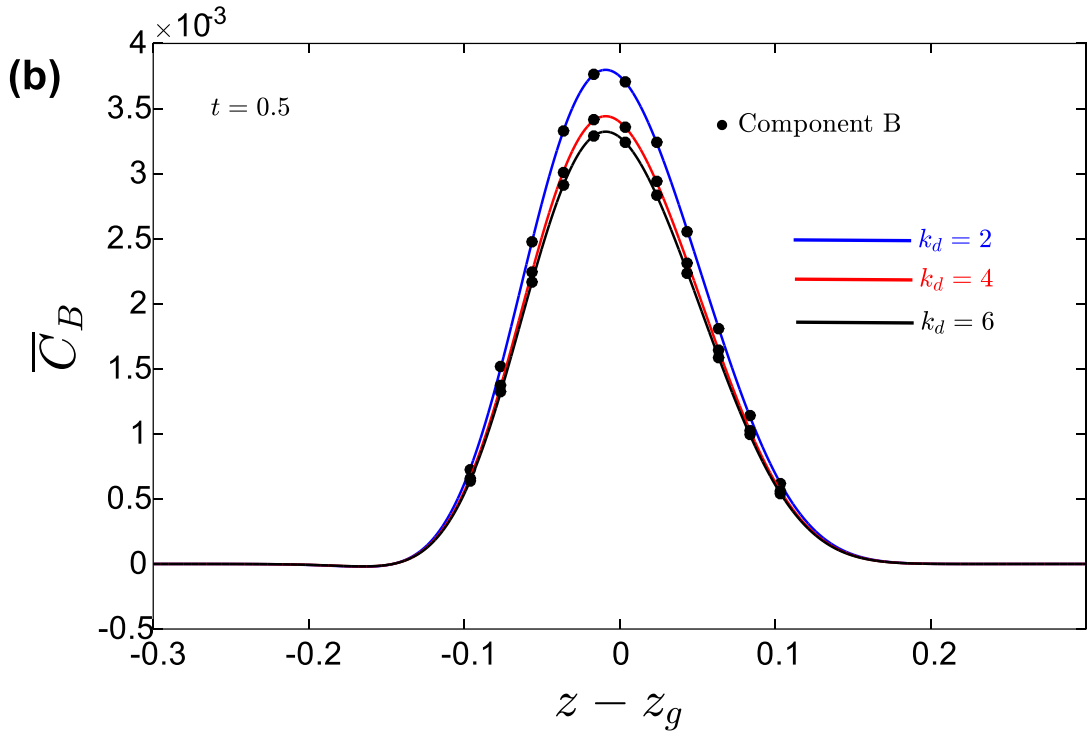

Fig. 10. Mean concentration distribution for species A and B for various k_d with fixed $\varepsilon_r = \varepsilon_k = 1$.

Finally, **Fig. 10a, b** visualizes the distributions for mean concentration distribution for species *A and B* for various k_d (distribution coefficient between two species) with fixed $\varepsilon_r = \varepsilon_k = 1$ (i.e., reversible reaction rates and irreversible degradation rates are equal for both species *A*, *B*). Non-Newtonian blood flow is again considered. Much higher orders of magnitude are observed for $\bar{C}_A$ magnitudes (**Fig. 10a**) relative to $\bar{C}_B$ magnitudes (**Fig. 10b**) at the same time instant (t = 0.5). However, while there is a distinct elevation in $\bar{C}_A$ magnitudes (**Fig. 10a**) with increase in k_d there is a notable (although less dramatic) depletion in $\bar{C}_B$ magnitudes.

5. Conclusions

A mathematical and computational study of the bi-component species transport (convective-diffusion) in Casson rheological blood flow with bulk chemical reaction through a two-dimensional rigid vessel has been presented. Two different bulk degradation reaction rates have been included for the dual species (pharmacological agents, *A*, *B*). The governing species concentration equations have been transformed to non-dimensional form with appropriate

boundary conditions. An analytical expression for axial velocity has been derived using a perturbation method. The decoupled convection-diffusion equations have been analyzed with the Aris – Barton approach, in which the p^{th} order moment of the general concentration is defined. The mean concentration of the species has been estimated using the first five concentration moments with the aid of fourth order Hermite polynomials. A finite difference method based on the Crank Nicholson implicit scheme has been adopted to solve numerically the nonlinear equation for the p^{th} order moment of the general concentration. A statistical analysis has also been conducted wherein coefficients of skewness and kurtosis have been computed to determine the symmetry and peaks of the concentration distribution. The present study has shown that increasing reversible transfer rate and irreversible bulk degradation result in a reduction in the total mass of the species over time. The mass of both species decreases with the increase of reversible transfer rate, although the mass of species *A* depletes faster than the mass of species *B.* With an increase of yield stress, the coefficient of skewness for the concentration distribution decreases and the distributions in all scenarios are positively skewed and tend to zero over time, implying that the distribution tends to symmetry over time. The kurtosis coefficient decreases over time from positive to negative values and eventually approaches zero. There is an initial critical time for each yield stress at which the kurtosis is zero; additionally, at large times, the kurtosis is also zero. The implication is that that the distribution of the species (drug) attains the Gaussian distribution at an initial critical time and also at large time. Mean concentration peaks for both species *A* and *B* are elevated with increasing yield stress, although magnitudes are significantly higher for species *A*. With increasing values of the distribution coefficient between two species, mean concentration peaks are elevated for species (component) *A* whereas they are depleted for species *B*, although substantially greater magnitudes are computed for species *B*. Good correlation of the skewness with earlier Newtonian results is achieved. The inclusion of non-Newtonian characteristics is generally demonstrated to substantially modify the mean concentration, skewness coefficient and kurtosis coefficient distributions compared with classical Newtonian models.

The results provide some useful insight into the bi-component drug transport in smaller vessel pharmacodynamics where hemo-rheology is important. Future studies may consider porous media effects and alternative non-Newtonian models e.g. Maxwell viscoelastic [60], Oldroyd-B [61] and Carreau [62] models and will be communicated imminently.

Acknowledgements:

The authors are thankful to the reviewers for their comments which have served to improve the article.

Conflict of interest:

The authors declare no competing interests.

References

[1] D. Dutta, Hydrodynamic Dispersion, in: D. Li (Ed.), Encyclopedia of Microfluidics and Nanofluidics, Springer US, Boston, MA, 2013: pp. 1–14. https://doi.org/10.1007/978-3-642-27758-0_660-3.

[2] P. Wang, Studies on the fluid mechanics and mass transfer in neural drug delivery, Cornell University, 2011. https://ecommons.cornell.edu/handle/1813/33599 (accessed September 25, 2021).

[3] M. Kleven, M.C. Melaaen, P.G. Djupesland, Computational fluid dynamics (cfd) applied in the drug delivery design process to the nasal passages: a review, J. Mech. Med. Biol. 12 (2012) 1230002. https://doi.org/10.1142/S0219519411004526.

[4] T.-W. Lee, K.-S. Bae, H.S. Choi, M.-J. Chern, Computational Simulations of Flow and Oxygen/Drug Delivery in a Three-Dimensional Capillary Network, ISRN Biomathematics. 2014 (2014) e359327. https://doi.org/10.1155/2014/359327.

[5] Y.-M.F. Goh, H.L. Kong, C.-H. Wang, Simulation of the delivery of doxorubicin to hepatoma, Pharm Res. 18 (2001) 761–770. https://doi.org/10.1023/A:1011076110317.

[6] S. Kalyanasundaram, V.D. Calhoun, K.W. Leong, A finite element model for predicting the distribution of drugs delivered intracranially to the brain, Am. J. Physiol. Regul. Integr. Comp. Physiol. 273 (1997) R1810–R1821. https://doi.org/10.1152/ajpregu.1997.273.5.R1810.

[7] C.S. Teo, W. Hor Keong Tan, T. Lee, C.-H. Wang, Transient interstitial fluid flow in brain tumors: Effect on drug delivery, Chem. Eng. Sci. 60 (2005) 4803–4821. https://doi.org/10.1016/j.ces.2005.04.008.

[8] W. Zhan, X.Y. Xu, A mathematical model for thermosensitive liposomal delivery of doxorubicin to solid tumour, J. Drug Delivery. 2013 (2013) 1–13. https://doi.org/10.1155/2013/172529.

[9] F. Brounéus, K. Karami, P. Beronius, L.-O. Sundelöf, Diffusive transport properties of some local anesthetics applicable for iontophoretic formulation of the drugs, Int. J. Pharm. 218 (2001) 57–62. https://doi.org/10.1016/S0378-5173(01)00612-3.

[10] J. Tripathi, B. Vasu, A. Dubey, R.S.R. Gorla, P.V.S.N. Murthy, O.A. Bég, V.R. Prasad, P. Saikrishnan, A review on recent advancements in the hemodynamics of nano-drug delivery systems, Nanosci. Technol.: Int. J. 11 (2020). https://doi.org/10.1615/NanoSciTechnolIntJ.2020033448.

[11] J. Aroesty, J.F. Gross, Convection and diffusion in the microcirculation, Microvasc. Res. 2 (1970) 247–267. https://doi.org/10.1016/0026-2862(70)90016-6.

[12] D.A. Siginer, D.D. Kee, R.P. Chhabra, Advances in the flow and rheology of non-Newtonian fluids, Elsevier, 1999.
[13] R.H. Haynes, A.C. Burton, Role of the non-Newtonian behavior of blood in hemodynamics, Am. J. Physiol. L. 197 (1959) 943–950. https://doi.org/10.1152/ajplegacy.1959.197.5.943.
[14] O.A. Bég, T.A. Bég, R. Bhargava, S. Rawat, D. Tripathi, Finite element study of transient pulsatile magneto-hemodynamic non-newtonian flow and drug diffusion in a porous medium channel, J. Mech. Med. Biol. 12 (2012) 1250081. https://doi.org/10.1142/S0219519412500819.
[15] F. De Vita, M.D. de Tullio, R. Verzicco, Numerical simulation of the non-Newtonian blood flow through a mechanical aortic valve: Non-Newtonian blood flow in the aortic root, Theor. Comput. Fluid Dyn. 30 (2016) 129–138. https://doi.org/10.1007/s00162-015-0369-2.
[16] N. Antonova, K. Tsiberkin, S. Podtaev, V. Paskova, I. Velcheva, N. Chaushev, Comparative study between microvascular tone regulation and rheological properties of blood in patients with type 2 diabetes mellitus, Clin. Hemorheol. Microcirc. 64 (2016) 837–844. https://doi.org/10.3233/CH-168000.
[17] A. Dubey, B. Vasu, O. Anwar Bég, R.S.R. Gorla, A. Kadir, Computational fluid dynamic simulation of two-fluid non-Newtonian nanohemodynamics through a diseased artery with a stenosis and aneurysm, Comput. Methods Biomech. Biomed. Eng. 23 (2020) 345–371. https://doi.org/10.1080/10255842.2020.1729755.
[18] P. Chaturani, R. Ponalagusamy, A study of non-newtonian aspects of blood flow through stenosed arteries and its applications in arterial diseases, Biorheol. 22 (1985) 521–531. https://doi.org/10.3233/BIR-1985-22606.
[19] B. Vasu, A. Dubey, O.A. Bég, R.S.R. Gorla, Micropolar pulsatile blood flow conveying nanoparticles in a stenotic tapered artery: Non-Newtonian pharmacodynamic simulation, Comput. Biol. Med. 126 (2020) 104025. https://doi.org/10.1016/j.compbiomed.2020.104025.
[20] D. Tripathi, A. Yadav, O.A. Bég, Electro-kinetically driven peristaltic transport of viscoelastic physiological fluids through a finite length capillary: Mathematical modeling, Math. Biosci. 283 (2017) 155–168. https://doi.org/10.1016/j.mbs.2016.11.017.
[21] A. Zaman, N. Ali, O.A. Bég, M. Sajid, Unsteady two-layered blood flow through a w-shaped stenosed artery using the generalized Oldroyd-B fluid model, The ANZIAM J. 58 (2016) 96–118. https://doi.org/10.1017/S1446181116000134.
[22] J.-H. Moh, Y.I. Cho, D.J. Cho, D. Kim, R.K. Banerjee, Influence of non-Newtonian viscosity of blood on microvascular impairment, Clin. Hemorheol. Microcirc. 57 (2014) 111–118. https://doi.org/10.3233/CH-141822.
[23] G.I. Taylor, Dispersion of soluble matter in solvent flowing slowly through a tube, Proc. R. Soc. London, Ser. A. 219 (1953) 186–203. https://doi.org/10.1098/rspa.1953.0139.
[24] W.N. Gill, A note on the solution of transient dispersion problems, Proc. R. Soc. London, Ser. A. 298 (1967) 335–339. https://doi.org/10.1098/rspa.1967.0107.
[25] W.N. Gill, R. Sankarasubramanian, Exact analysis of unsteady convective diffusion, Proc. R. Soc. London, Ser. A. 316 (1970) 341–350. https://doi.org/10.1098/rspa.1970.0083.
[26] J.B. Grotberg, B.V. Sheth, L.F. Mockros, An analysis of pollutant gas transport and absorption in pulmonary airways, J. Biomech. Eng. 112 (1990) 168–176. https://doi.org/10.1115/1.2891168.
[27] O.A. Cirpka, P.K. Kitanidis, Numerical evaluation of solute dispersion and dilution in unsaturated heterogeneous media, Water Resour. Res. 38 (2002) 2-1-2–15. https://doi.org/10.1029/2001WR001262.

[28] R.K. Dash, G. Jayaraman, K.N. Mehta, Shear augmented dispersion of a solute in a Casson fluid flowing in a conduit, Ann. Biomed. Eng. 28 (2000) 373–385. https://doi.org/10.1114/1.287.
[29] S. Barik, D.C. Dalal, Multi-scale analysis for concentration distribution in an oscillatory Couette flow, Proc. R. Soc. London, Ser. A. 475 (2019) 20180483. https://doi.org/10.1098/rspa.2018.0483.
[30] K.G. Mann, Biochemistry and physiology of blood coagulation, Thromb. Haemost. 82 (1999) 165–174. https://doi.org/10.1055/s-0037-1615780.
[31] F. Shen, R.R. Pompano, C.J. Kastrup, R.F. Ismagilov, Confinement regulates complex biochemical networks: initiation of blood clotting by "Diffusion Acting," Biophys. J. 97 (2009) 2137–2145. https://doi.org/10.1016/j.bpj.2009.08.004.
[32] D.J. Singel, J.S. Stamler, Chemical physiology of blood flow regulation by red blood cells:, Annu. Rev. Physiol. 67 (2005) 99–145. https://doi.org/10.1146/annurev.physiol.67.060603.090918.
[33] B. Zhao, K. Poonit, X. Zhou, C. Yao, C. Sun, H. Yan, The effect of chemical hemodynamic regulation on the survival of arterialized venous flaps, Journal of Plastic Surgery and Hand Surgery. 53 (2019) 83–88. https://doi.org/10.1080/2000656X.2018.1550418.
[34] R. Hennig, K. Pollinger, A. Veser, M. Breunig, A. Goepferich, Nanoparticle multivalency counterbalances the ligand affinity loss upon PEGylation, J. Controlled Release. 194 (2014) 20–27. https://doi.org/10.1016/j.jconrel.2014.07.062.
[35] N. Mackman, Triggers, targets and treatments for thrombosis, Nature. 451 (2008) 914–918. https://doi.org/10.1038/nature06797.
[36] B. Furie, B.C. Furie, Thrombus formation in vivo, J. Clin. Investig. 115 (2005) 3355–3362. https://doi.org/10.1172/JCI26987.
[37] J.J. Hathcock, Flow effects on coagulation and thrombosis, Arterioscler Thromb Vasc. Biol. 26 (2006) 1729–1737. https://doi.org/10.1161/01.ATV.0000229658.76797.30.
[38] M.W. Lau, C.O. Ng, On the early development of dispersion in flow through a tube with wall reactions, in: F.G. Zhuang, J.C. Li (Eds.), New Trends in Fluid Mechanics Research, Springer, Berlin, Heidelberg, 2009: pp. 670–673. https://doi.org/10.1007/978-3-540-75995-9_224.
[39] C.-O. Ng, Dispersion in steady and oscillatory flows through a tube with reversible and irreversible wall reactions, Proc. R. Soc. London, Ser. A. 462 (2006) 481–515. https://doi.org/10.1098/rspa.2005.1582.
[40] S. Paul, B.S. Mazumder, Transport of reactive solutes in unsteady annular flow subject to wall reactions, Eur. J. Mech. B. Fluids. 28 (2009) 411–419. https://doi.org/10.1016/j.euromechflu.2008.09.003.
[41] S. Paul, B.S. Mazumder, Effects of nonlinear chemical reactions on the transport coefficients associated with steady and oscillatory flows through a tube, Int. J. Heat Mass Transfer. 54 (2011) 75–85. https://doi.org/10.1016/j.ijheatmasstransfer.2010.08.028.
[42] B.S. Mazumder, S. Paul, Dispersion of reactive species with reversible and irreversible wall reactions, Heat Mass Transfer. 48 (2012) 933–944. https://doi.org/10.1007/s00231-011-0920-7.
[43] A.K. Roy, O.A. Bég, A.K. Saha, J.V.R. Murthy, Taylor dispersion in non-Darcy porous media with bulk chemical reaction: a model for drug transport in impeded blood vessels, J. Eng. Math. 127 (2021) 24. https://doi.org/10.1007/s10665-021-10120-8.
[44] A.K. Roy, A.K. Saha, S. Debnath, Unsteady convective diffusion with interphase mass transfer in Casson liquid, Period. Polytech. Chem. Eng. 62 (2018) 215–223. https://doi.org/10.3311/PPch.10328.

[45] A.K. Roy, O.A. Bég, Mathematical modelling of unsteady solute dispersion in two-fluid (micropolar-Newtonian) blood flow with bulk reaction, Int. Commun. Heat Mass Transfer. 122 (2021) 105169. https://doi.org/10.1016/j.icheatmasstransfer.2021.105169.
[46] L. Zeng, Y.J. Zhao, B. Chen, P. Ji, Y.H. Wu, L. Feng, Longitudinal spread of bicomponent contaminant in wetland flow dominated by bank-wall effect, J. Hydrol. 509 (2014) 179–187. https://doi.org/10.1016/j.jhydrol.2013.11.015.
[47] F. Gjetvaj, A. Russian, P. Gouze, M. Dentz, Dual control of flow field heterogeneity and immobile porosity on non-Fickian transport in Berea sandstone, Water Resour. Res. 51 (2015) 8273–8293. https://doi.org/10.1002/2015WR017645.
[48] P. Ganesan, R. Soundararajan, U. Shanmugam, V. Ramu, Development, characterization and solubility enhancement of comparative dissolution study of second generation of solid dispersions and microspheres for poorly water soluble drug, Asian J. Pharm. Sci. 10 (2015) 433–441. https://doi.org/10.1016/j.ajps.2015.05.001.
[49] L.S. Taylor, G. Zografi, Spectroscopic characterization of interactions between PVP and indomethacin in amorphous molecular dispersions, Pharm. Res. 14 (1997) 1691–1698. https://doi.org/10.1023/A:1012167410376.
[50] G.R. Lloyd, D.Q.M. Craig, A. Smith, A calorimetric investigation into the interaction between paracetamol and polyethlene glycol 4000 in physical mixes and solid dispersions, Eur. J. Pharm. Biopharm. 48 (1999) 59–65. https://doi.org/10.1016/S0939-6411(99)00022-3.
[51] H. Berthold, A. Just, H.R. Kirchheim, H. Ehmke, Interaction Between Nitric Oxide and Endogenous Vasoconstrictors in Control of Renal Blood Flow, Hypertension. 34 (1999) 1254–1258. https://doi.org/10.1161/01.HYP.34.6.1254.
[52] J. Rana, P.V.S.N. Murthy, Solute dispersion in pulsatile Casson fluid flow in a tube with wall absorption, J. Fluid Mech. 793 (2016) 877–914. https://doi.org/10.1017/jfm.2016.155.
[53] N.G. Barton, On the method of moments for solute dispersion, J. Fluid Mech. 126 (1983) 205–218. https://doi.org/10.1017/S0022112083000117.
[54] S. Debnath, S. Paul, A.K. Roy, Transport of reactive species in oscillatory annular flow, J. Appl. Fluid Mech. 11 (2018) 405–417. https://doi.org/10.29252/jafm.11.02.27849.
[55] A.K. Roy, A.K. Saha, S. Debnath, Hydrodynamic dispersion of solute under homogeneous and heterogeneous reactions, Int. J. Heat Technol. 37 (2019) 387–397. https://doi.org/10.18280/ijht.370203.
[56] B.S. Mazumder, S.K. Das, Effect of boundary reaction on solute dispersion in pulsatile flow through a tube, J. Fluid Mech. 239 (1992) 523–549. https://doi.org/10.1017/S002211209200452X.
[57] A.K. Roy, A.K. Saha, S. Debnath, On dispersion in oscillatory annular flow driven jointly by pressure pulsation and wall oscillation, J. Appl. Fluid Mech. 10 (2017) 1487–1500. https://doi.org/10.18869/acadpub.jafm.73.242.27702.
[58] S. Debnath, A.K. Saha, B.S. Mazumder, A.K. Roy, Dispersion phenomena of reactive solute in a pulsatile flow of three-layer liquids, Phys. Fluids. 29 (2017) 097107. https://doi.org/10.1063/1.5001962.
[59] P. Wang, G.Q. Chen, Basic characteristics of Taylor dispersion in a laminar tube flow with wall absorption: Exchange rate, advection velocity, dispersivity, skewness and kurtosis in their full time dependance, Int. J. Heat Mass Transfer. 109 (2017) 844–852. https://doi.org/10.1016/j.ijheatmasstransfer.2017.02.051.

[60] H. Waqas, M. Imran and M.M. Bhatti, Influence of bioconvection on Maxwell nanofluid flow with the swimming of motile microorganisms over a vertical rotating cylinder. Chinese Journal of Physics. 2020 Volume 68, December 2020, Pages 558-577.

[61] S. Rana, R. Mehmood and M.M. Bhatti, Bioconvection oblique motion of magnetized Oldroyd-B fluid through an elastic surface with suction/injection, Chinese Journal of Physics 73 (2021) 314-330.

[62] A. Shahid, M.M. Bhatti, R. Ellahi and K.S. Mekheimer, Numerical experiment to examine activation energy and bi-convection Carreau nanofluid flow on an upper paraboloid porous surface: Application in solar energy. Sustainable Energy Technologies and Assessments, 52, 102029.